Synthesis of Dopant-Segregated Tin-Doped Indium Oxide (ITO) Nanocrystals

by

Ashley Bird

Stephen Gibbs

Dr. Delia Milliron

McKetta Department of Chemical Engineering

The University of Texas at Austin

Spring 2018

Abstract

The use of a localized surface plasmon resonance (LSPR) in nanostructures has been explored in sensing, spectroscopy, and smart window applications. Furthermore, the ability to synthetically or post-synthetically tune the LSPR frequency has made these materials an increasingly interesting area of study. Metal oxide nanocrystals (NCs) exhibit an LSPR frequency in the infrared region, making them useful for molecular sensing. LSPR also results in an enhanced electric field near the NC surface. The near-field enhancement (NFE) can improve sensing, but the presence of a depletion layer at the NC surface reduces NC sensitivity. By segregating dopants to the surface of the NC, the depletion layer can be reduced, thereby improving NC sensitivity to its surroundings. To study the impact of radial dopant distribution in the NC, it is necessary to independently maintain a high degree of synthetic control over the dopant concentration and NC size.

Synthetic control has recently been demonstrated for tin-doped indium oxide (ITO) nanocrystals. Using a slow growth synthesis method relying on the rapid esterification of metal oleate and subsequent condensation reaction, independent control over the size, doping level, and radial dopant distribution of tin-doped indium oxide (ITO) nanocrystals was achieved. Two series of NCs were synthesized: a core series with constant ITO shell thickness and a shell series with constant indium oxide core volume.

Size and polydispersity were determined by scanning transmission electron microscopy (STEM), and dopant segregation was verified by x-ray photoelectron spectroscopy (XPS) and inductively coupled plasma optical emission spectroscopy (ICP-OES). The simulated optical spectra of the core/shell NCs revealed a change in intensity due to the changing volume fraction of ITO. However, a dual-mode in the LSPR was also shown, indicating further investigation is necessary. These materials have potential in dynamic sensors due to the ability to post-synthetically modulate the LSPR frequency and improved sensitivity. A method to extract the optical and electronic properties of the core/shell NCs is described. SCOUT, an optical spectra simulation software, was used to build models that fit experimental spectra at various applied biases in order to extract optical and electronic properties.

Table of Contents

List of Figures and Tables

Figures:

Tables:

Preface

Plasmonic materials are an exciting area of study. The light-matter interactions result in interesting optoelectronic properties that can be utilized in sensors, smart windows, solar cells, and enhanced spectroscopy. Metal oxide nanocrystals (NCs) exhibit a localized surface plasmon resonance (LSPR), which resonates in the infrared region. Due to the inherently lower free electron concentration compared to metals, these materials allow smaller scale nanostructures with higher packing, yet the near-field enhancement is comparable to metals. The ability to modulate the LSPR frequency over a wide range by synthetic and post-synthetic methods, metal oxide NCs are advantageous in applications, such as dynamic sensing technologies, which rely on the NC interacting with molecules near the NC surface. Challenges to implementing these materials results from the presence of a depletion layer at the NC surface that reduce sensitivity to external stimuli. To improve sensitivity, research in understanding the relationship between the depletion layer and other material properties is necessary.

Acknowledgements

I would like to thank Stephen Gibbs, who was an incredible mentor throughout this project, providing encouragement and advice when I needed it.

I would also like to thank Prof. Delia Milliron, who has been supportive of my interests and goals, as well as the people in the Milliron group, both past and present, for welcoming me into the lab for the past two years. Even through small interactions, I could tell that they not only have a wealth of information to share but are eager to provide help.

Finally, I would like to thank my friends and family. I would like to give special thanks to Erica Mason, who has been a pillar of support throughout this challenging process while she worked on her own thesis.

Chapter 1. Introduction

1.1 Doped metal oxide nanocrystals

Degenerately doped metal oxide nanocrystals (NCs) are semiconductors that exhibit a localized surface plasmon resonance (LSPR). The dopants donate free electrons to the metal oxide NC. Upon incident electromagnetic radiation, the free electrons are excited and oscillate, resulting in a plasmonic response. For a bulk material, the surface plasmon propagates along the material and dielectric interface. However, in nanostructures, the plasmon response is confined to the volume of the material. The ability to tune the LSPR frequency, synthetically or post-synthetically, over a wide range has made plasmonic nanomaterials the subject of research for applications in sensors,[1-5] surface enhanced spectroscopy,[1,2,5-7] and smart windows.[1,8]

The LSPR can be tuned by manipulating the carrier concentration during synthesis by varying the doping concentration where increased doping – and therefore increased carrier concentration – results in blue shifts in the LSPR frequency.[9] Post-synthetic modulation has been demonstrated by changing the free electron concentration through electrochemical,[10] photochemical,[11-13] and chemical[4] means. While metal NCs also exhibit LSPR, the resonant frequency occurs at higher energies due to the inherently larger carrier concentration, typically in the visible light range.[14] Metal oxide NCs, on the other hand, exhibit LSPR in the IR region. Figure 1.1 shows the resonance energies of various metals and metal oxides.[14] The extent of modulation for metal oxide NCs is much larger for metal oxides than for metals.[10]

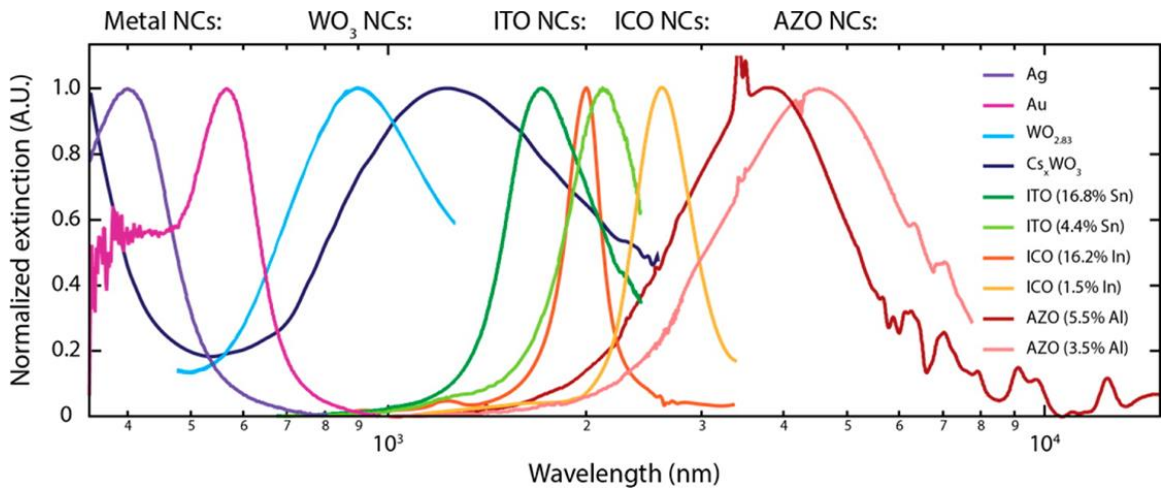

Figure 1.1 Normalized spectra of various NCs. Metal NCs have higher LSPR frequencies in the visible light region compare to metal oxide NCs, which exhibit LSPR in the infrared region.[14]

However, the ability to tune the LSPR frequency of metal nanostructures to lower frequencies in the IR region is limited to changes in morphology and increases in sizes.[3,15-16] Metal oxides NCs, on the other hand, have lower carrier concentrations compared to metals, leading to an LSPR frequency in the IR while maintaining control over the NC size and geometry. Thus, metal oxide NCs are desirable in applications required LSPR frequencies in the IR region. Since molecular vibrations occur in the IR, these materials have been proposed in vibrational spectroscopy. Additionally, sensor response can be improved with higher packing densities achieved by using metal oxide NCs as opposed to larger metal nanostructures.

Through molecular vibration-LSPR coupling, metal oxide NCs can be used to detect the presence of target molecules. The plasmonic response strengthens the electric field near the NC surface, and this near-field enhancement (NFE) enables coupling between the LSPR and molecular vibrations. Therefore, greater NFE improves sensitivity in sensing. As NFE is greatest at the LSPR frequency, it is important for the LSPR frequency to be in the IR region. However, recent studies have reported the formation of a depletion layer at the NC surface, reducing NFE.[17] To improve the NC sensitivity, it is necessary to reduce the effects of depletion. Recent literature has shown that manipulating the radial dopant distribution in metal oxide NCs can reduce the depletion layer thickness, thereby improving NFE.[18] This work focuses on segregating dopants to the NC surface to improve NC sensitivity.

To study the impact of dopant distribution on the depletion layer, tin-doped indium oxide (ITO) is used as the model system. ITO is a well-studied material used commercially in optical coatings, displays, and windows. Synthetic control over NC size, doping concentration, and dopant distribution has also been demonstrated in literature.[19-21] This work discusses the synthesis, optical properties, and electronic properties of dopant-segregated ITO NCs.

1.2 Optical properties

The optical properties of metal oxide NCs are determined by its dielectric function. In literature, the complex dielectric function using the Drude model for a free electron gas is often applied to semiconductors.[1,8-9,14,21-24,26] The Drude model is given by Equation 1.1:

$$\varepsilon(\omega) = \varepsilon_{\infty} - \frac{\omega_p^2}{\omega^2 + i\omega\Gamma} \qquad \text{(Equation 1.1)}$$

where ε_{inf} is the high frequency dielectric constant, ω_p is the plasma frequency, and Γ is the damping coefficient. Damping can arise from different types of electron scattering: surface scattering, electron-electron scattering, electron-phonon scattering, radiative energy loss, and ionized impurity scattering. Scattering affects the optical response of NCs by changing the width or symmetry the plasmon peak.[9,14]

The LSPR peak frequency is directly proportional to the plasma frequency, which depends on the free carrier concentration, as shown by Equation 1.2:

$$\omega_{LSPR} \propto \omega_p = \sqrt{\frac{ne^2}{\varepsilon_0 m^*}} \qquad \text{(Equation 1.2)}$$

where n is the free electron concentration, e is the elementary electronic charge, m^* is the effective electron mass, and ε_0 is the permittivity of free space. Increasing the doping levels in the NCs increases free electron concentration, resulting in an increase in the plasma frequency and blue shift in the LSPR frequency. Similarly, reducing the dopant concentration leads to a red shift in the LSPR frequency.

The LSPR absorption cross section (σ_A) can be calculated using the dielectric function of the material, as shown by Equation 1.3:

$$\sigma_A = 4\pi k r^3 Imag\{\frac{\varepsilon(\omega)-\varepsilon_m}{\varepsilon(\omega)+2\varepsilon_m}\} \qquad \text{(Equation 1.3)}$$

where $k = \sqrt{\varepsilon_m}\ \omega/c$, r is the NC radius, and $\varepsilon(\omega)$ is taken from the Drude model. Equation 1.3 is derived from Mie Theory, which assumes that the NC is much smaller than the wavelength of light. Additionally, the NCs are assumed to be non-interacting. From the

LSPR absorption cross section, the Beer-Lambert law can be used to determine the total absorbance (A) of the NCs, as given by Equation 1.4:

$$A = \frac{N\sigma_A L}{\log(10)} \qquad \text{(Equation 1.4)}$$

where N is the number density (number of nanoparticles per unit volume) and L is the path length of the cell.

Manipulating the radial dopant distribution of plasmonic NCs – and therefore, the carrier concentration – has been shown to impact the optical properties, including the LSPR line shape and scattering.[9,21] In addition to the effects on the optical properties of the NCs, the dopant distribution is expected to impact the electronic properties.

1.3 Electronic properties

Doped metal oxide NCs also have interesting electronic properties due to the contribution of free electrons by dopants. In an undoped metal oxide NC, the fermi level is below the conduction band minimum. The fermi level is the highest energy level of electrons in a material. N- type dopants donate free electrons to the NCs, resulting in the fermi level shifting to energies higher than that of the conduction band, as shown in

Figure 1.2. The electrons can populate the conduction band, and the resulting delocalized charges resonate upon incident radiation, creating the plasmonic response.

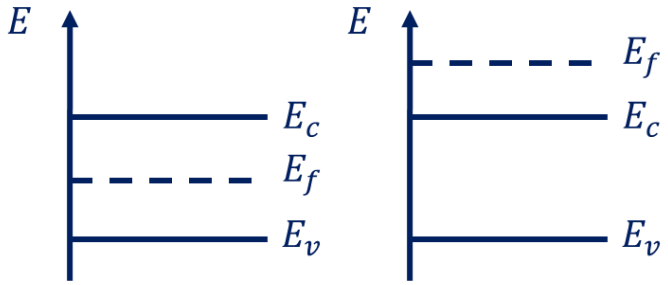

Figure 1.2 Energy level diagrams. Diagrams for (left) undoped metal oxide NCs and (right) and doped metal oxide NCs.

In the bulk material, the band gap can be illustrated by Figure 1.2a and 1.2b. However, on the nanoscale, the surface effects are not negligible. Surface states that lie energetically below the fermi level of the NC can pin the NC fermi level, resulting in conduction band bending. For metal oxide NCs, surface states result from surface-bound molecules, surface trap states, and surface defects.[24]

The lowered fermi level at the surface causes the electrons to migrate from the NC to the surrounding media. The resulting space-charge region opposes further migration of electrons so that the carrier concentration at the NC surface is less than the internal concentration. The reduced electron concentration at the surface is the depletion layer. In bulk materials, effects of this layer may be neglected. However, the length scale of the depletion layers is not negligible for nanoscale structures, and the depletion layer impacts

the material properties of the NCs.[18,24] Figure 1.3 shows electron concentration and band gap profiles for a NC with and without depletion.[18] For a uniformly doped NC, the electron concentration depletes near the surface, and the conduction band bends upward at the surface. For a core/shell NC with dopants segregated to the shell, the extent of depletion is reduced, as indicated by the concentration profile. In the band gap profile, the conduction band bends but remains below the fermi level.

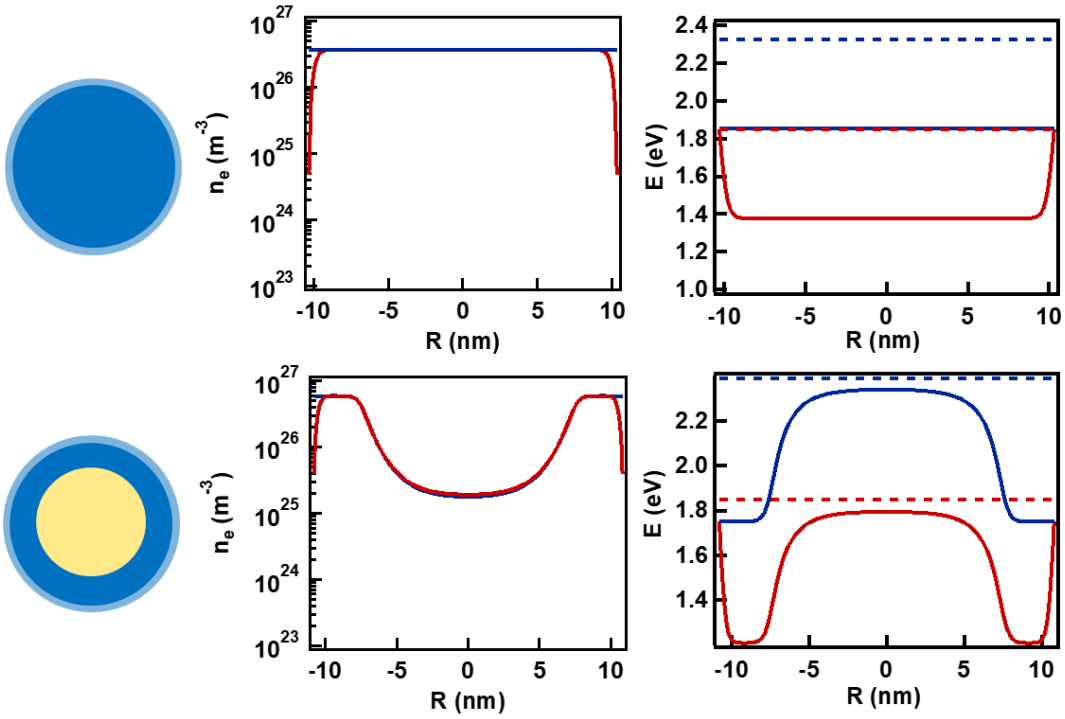

Figure 1.3 Electron concentration and energy level profiles. Electron concentration profiles are shown on the left, and energy level profiles are on the right. Profiles for (top) uniformly doped and (bottom) dopant-segregated NCs. Blue lines indicate the profiles without depletion, and red lines are profiles with depletion.[18]

As stated previously, the plasmonic response of the NC results in NFE at the surface. Coupling between the LSPR and molecular vibrations is enabled by NFE and allows molecular sensing.[16] Greater NFE improves NC sensitivity to surrounding media. Thus, it is advantageous in sensing technology to achieve higher NFE. However, recent work has shown that NFE is reduced by depletion.[17] Since dopant segregation to the NC surface has been shown to reduce depletion, it follows that the NFE can also be improved by dopant segregation.[18] Therefore, dopant-segregated metal oxide NCs can provide a material with improved sensitivity to external stimuli, improving sensing technology.

Chapter 2: Synthesis

2.1 Growth mechanism

To investigate the impact of dopant segregation on the sensitivity of the NC, independent synthetic control over the size and radial dopant distribution is necessary. Traditional methods relied on the thermal degradation of metal precursors.[25] These methods required high temperatures (>300 C), using either a "hot injection" or a "heat up" method. However, these methods are limited in the degree of size and dopant control; a high degree of independent sub-nanometer size and doping level control is not achieved.[20,25] Recent developments in the alcoholysis of metal carboxylates have improved synthetic control.

Ito et al. recently developed a slow growth synthesis utilizing the ability of certain metals to catalyze the esterification of a carboxylic acid and alcohol.[19] They demonstrated controlled synthesis of several metal oxide NCs, including indium oxide (IO) and ITO NCs. The synthesis of core/shell NCs using γ-Fe_2O_3/MnO and ZnO/β-Ga_2O_3 was also demonstrated. Independent control over the size and dopant distribution of ITO was later demonstrated by Jansons et al.[20] A procedure for synthesizing core/shell ITO/IO NCs with precise size control was described, but consideration for the reaction temperature was necessary. The impact of dopant segregation on the LSPR and damping was also later explored.[2] This study showed that dopant segregation to the NC core reduced scattering. As the synthesis procedure provides the necessary control over size and dopants, the procedure was adapted in this study.

During the synthesis, metal carboxylate reacts with oleyl alcohol, a high boiling point solvent, in an esterification reaction. The metal catalyzes the reaction between the deprotonated carboxylic acid and alcohol, producing ester and a metal hydroxide, the reactive species for NC growth. When the metal hydroxide species reaches a high enough concentration, the metal hydroxides react with each other in a condensation reaction, producing water and growing the metal oxide NC. This procedure works for multiple metals, starting from the common metal acetate forms.[19] However, due to the poor solubility of indium (iii) acetate in oleyl alcohol below 245 C, the acetate ligand is exchanged with oleic acid to form indium oleate. Indium oleate is then injected into hot oleyl alcohol. A slow injection rate is used to prevent precipitation of solid metal oxides.

Furthermore, water and hydroxyls have been shown to stabilize the {100} facets of indium oxide, inhibiting the growth of spherical NCs.[19] Previous results indicated that water condensation results in metal oxide precipitation. Using a continuous flow of inert nitrogen, water vapor produced by the condensation reaction is removed.

The reaction scheme is illustrated in Figure 2.1.[20] The oleyl alcohol and metal oleate undergo rapid esterification, producing metal hydroxides which react in a condensation reaction, resulting in either NC nucleation or continued growth of NC. In the case of continued growth, the oleic acid ligand on the NC surface is converted to an ester, leaving a hydroxyl on the NC available to react with the metal hydroxides. The NC is able to continue growing due to the surface ligands unless the surface is passivated.

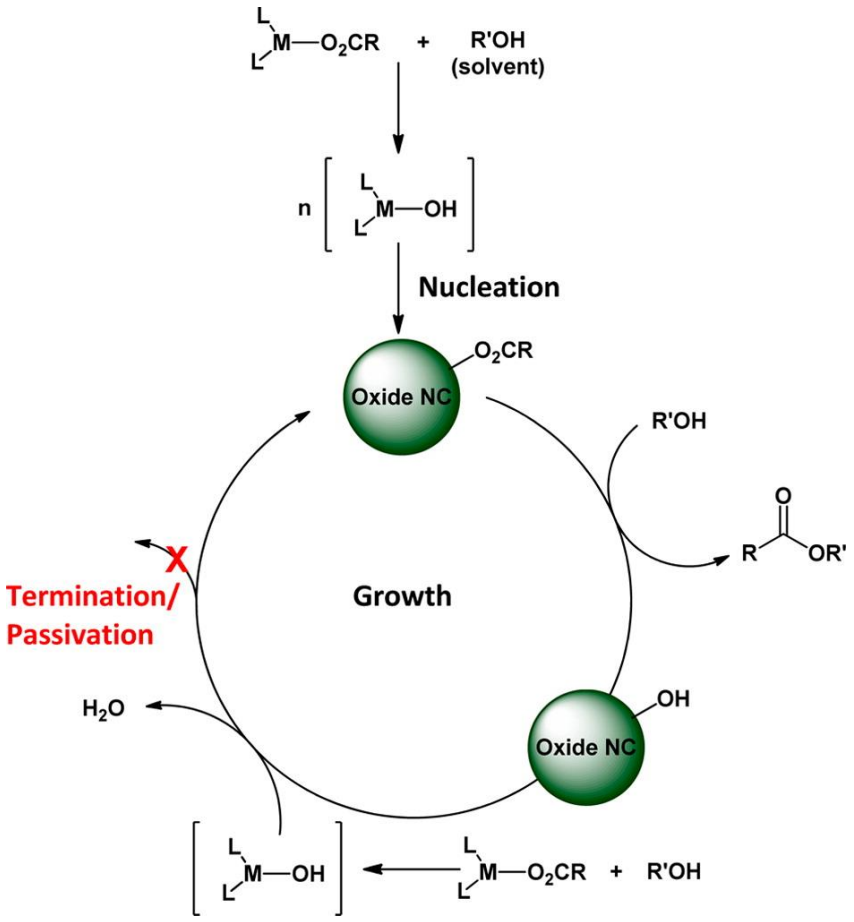

Figure 2.1 Reaction scheme for slow-growth metal oxide nanocrystals. The metal carboxylate undergoes esterification with the alcohol, leaving hydroxyls on the metal. Metal hydroxyls react with each other in a condensation reaction, leading to nucleation. The carboxylate ligands on the NC surface react further with the alcohol solvent to form the reactive species, which then undergoes condensation with other metal hydroxyls to grow the NC.[20]

This method allows for continuous growth with a linear relationship to the amount of metal precursor added. Additionally, the NCs can continue growing even after cooling

and washing as long as the surface is not passivated. XPS of these NCs indicates that the surface of the NCs are stabilized by oleic acid ligands, which allows for continued growth.[20] This slow growth method allows control over the size of the NC independent of the dopant concentration.

For doped metal oxide NCs, it is important to consider the reactivity of the metal precursors to achieve control over the dopant distribution. By this esterification process, the reactivities for tin (iv) acetate and indium (iii) acetate are similar, allowing control over the doping levels by simply modifying the feed ratio.[20] Core/shell synthesis was also demonstrated with control over the radial distribution of tin. To make ITO/IO core/shell NCs, the ITO precursor was injected into oleyl alcohol followed by the injection of the IO precursor. The successful segregation of tin to the core of the NC was determined through ICP and XPS. It is important to note that the shell precursors were added directly to the NC solution without purification of the NC cores. When synthesizing core/shell structures, secondary nucleation upon injection of the "shell" material into the reaction flask is another concern. However, this was not reported.

2.2 Synthesis of core/shell structures

The goal of this study requires segregation of dopants to the surface of the NC, so this study focuses on the synthesis of IO cores with ITO shells. To segregate the dopants to the surface of the NCs, the procedure developed by the Hutchison group was adapted.

To synthesize the metal precursors, indium (III) acetate and the desired amount of dopant tin (IV) acetate are added to oleic acid and degassed to remove water using a Schlenk line. The precursor solution is then heated to 150 C and soaked for 2 hours. During this reaction, the metal acetate is converted to metal oleate at (roughly) the same ratio as the feed composition. To obtain more control and reduce the influence of hydroxyls on NC growth, both the indium oleate solution and oleyl alcohol were degassed to remove water.

To form IO cores, the indium oleate is injected at 0.2 mL/min into oleyl alcohol at 290 C. After cooling, the NCs are washed to remove any remaining unreacted metal precursor in solution and then redispersed in hexane. In the previous method, the shell material was added directly to the reaction solution with the NC cores. By removing any remaining reactive species, more defined segregation of tin to the NC shell compared to the previous method is expected. To form the NC shell, IO cores in hexane are added to oleyl alcohol, and then the solution is degassed. It is important to provided heating during this degas because the endothermic evaporation of hexane can cool the oleyl alcohol to a viscous solution. The reaction solution is then heated to 290 C, and the ITO precursor is injected using the same method for the IO precursor. NCs are collected and purified by washing with IPA and redispersing in hexane before characterization and analysis. Figure 2.2 illustrates this process for growing core/shell NCs.

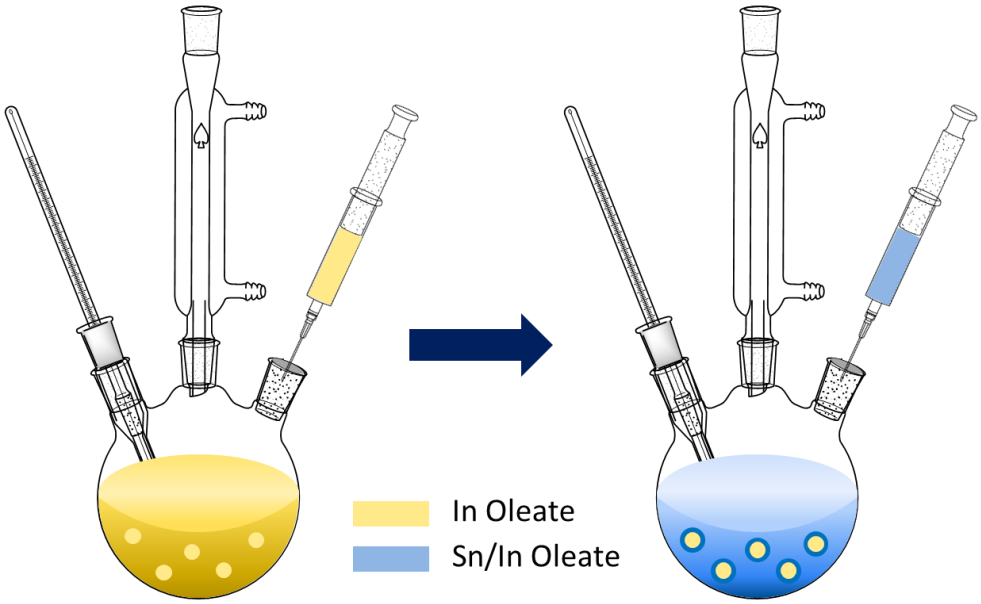

Figure 2.2 Instrumentation and process for growing core/shell NCs. After degassing the oleyl alcohol and heating to 290 C, the IO precursor is injected into Flask 1 (left) at 0.2 mL/min. The cores are removed from the flask and washed to remove any remaining reactive species. To grow shells on the NCs, the cores are added to fresh oleyl alcohol heated to 290 C in Flask 2 (right). The ITO precursor is then injected to grow the NC shell at 0.2 mL/min.

2.3 Characterization of core/shell nanocrystals

To study the effect of radial dopant distribution, two series of IO/ITO core/shell NCs were synthesized: a core series and a shell series. Tin concentration in ITO for all NCs was held constant at 5%. In the core series, the radius of the IO core is increased while the ITO shell thickness is held constant, which allows study of NCs with increasing IO

volume fraction. Conversely, in the shell series, the IO core radius is held constant while the ITO shell thickness is increased, which allows study of NC with increasing ITO volume fraction. Table 2.1 gives the core and shell sizes for synthesized samples.

Shell Series		
Core Diameter (nm)	Shell Thickness (nm)	Polydispersity (%)
15.8	1.9	5.1
16.5	2.5	4.7
16.1	3.4	5.2
16.3	4.1	4.9

Core Series		
Core Diameter (nm)	Shell Thickness (nm)	Polydispersity (%)
11.1	3	5.3
13	3.2	4.6
16.1	3.4	5.2
17.6	2.7	3.9

Table 2.1 Sample core and shell sizes. The core series had varying core diameters and shell thicknesses of approximately 3 nm. The shell series had core diameters of approximately 16 nm and varying shell thicknesses. The polydispersity was less than 6% for all samples.

As the IO core radius is increased, it is expected that the properties of the NCs to approach properties of undoped IO NCs. Similarly, as the ITO shell thickness is increased, the NCs properties are expected to approach the behavior of uniformly doped ITO NCs. Although the total volume of the compared NCs is different within the series, optical measurements

are normalized to the NC volume. Doing so allows easier synthetic control over the dopant segregation.

NC sizing was performed using scanning transmission electron microscopy (STEM) images. The segregation of dopants to the surface of the NC is expected to impact the extent of depletion. Therefore, it is necessary to measure the size of the IO cores and ITO shells. The images were analyzed in ImageJ to determine the both the size and polydispersity of the NCs. Before imaging, NCs were cleaned by repeatedly crashing the NCs with a polar solvent and resuspending in hexane, a volatile nonpolar solvent. Washing removes the organic ligands, which burn more quickly in STEM and make imaging more difficult.

Figure 2.3 gives sample STEM images with the resulting size distributions. Core NCs were unimodal. In some cases, the size distribution of the NCs after shelling were bimodal. This is attributed to secondary nucleation arising from ITO injected into a solution containing washed IO NC cores, which potentially have reduced reactive ligand coverage on the NC surface. However, the shelled NCs are larger than the ITO secondary NCs and, therefore, require less antisolvent to crash out of solution during washing than the NCs from secondary nucleation. As a result, the secondary NCs can be removed during washing and the larger IO/ITO core/shell NCs can be collected. The collected IO/ITO core/shell NCs are then unimodal.

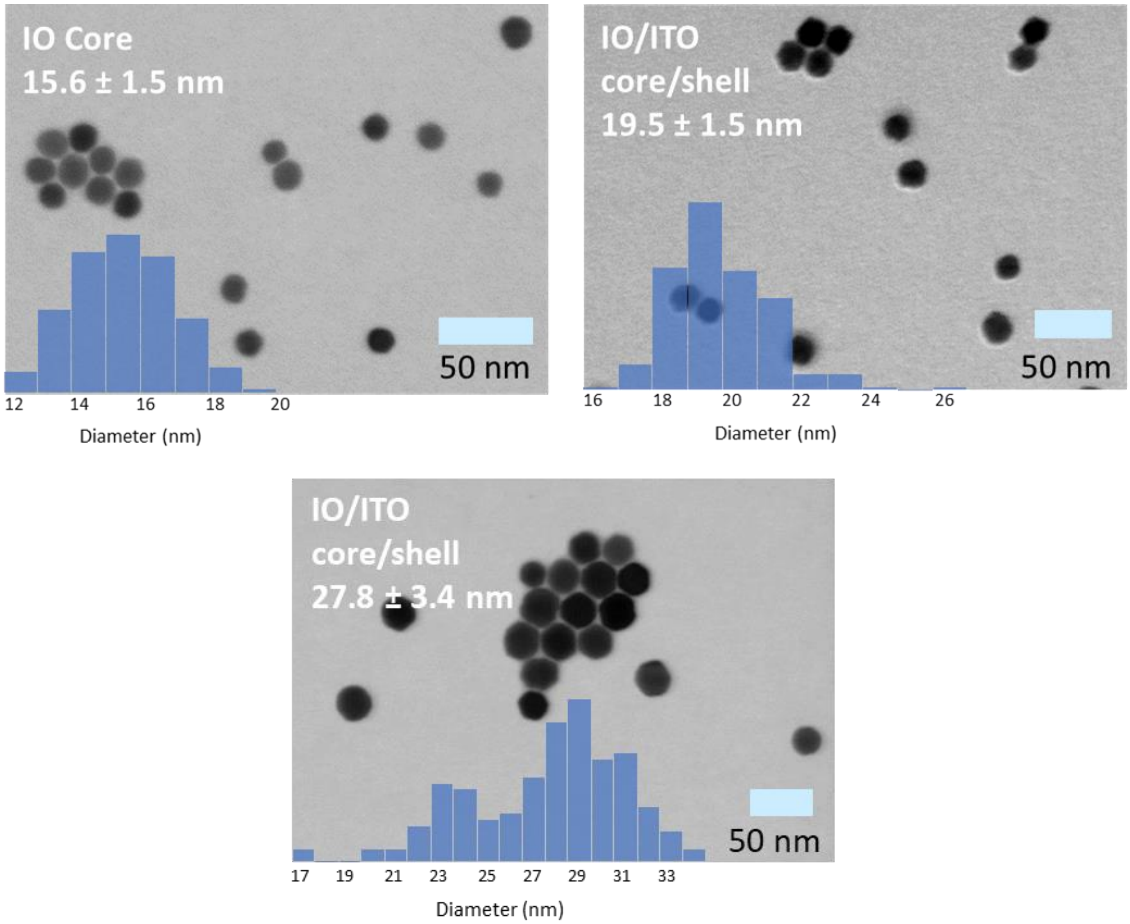

Figure 2.3 STEM images of core/shell NCs. Images of core and core/shell NCs show spherical particles. The IO cores (top left) were used to synthesized both sets of the core/shell NCs. (top right) The core/shell NCs are unimodal while another batch of NCs (bottom) had a bimodal distribution due to the secondary nucleation. The core/shell NCs can be isolated by washing.

To verify the dopants were confined in the shell and did not migrate within the NC, inductively coupled plasma (ICP) and x-ray photoelectron spectroscopy (XPS) analysis were used. ICP allows determination of the overall tin and indium concentration in the NCs. However, XPS is a surface-sensitive technique that allows determination of

chemical composition at the surface. For IO/ITO core/shell structures, higher concentrations of tin are expected to be measured by XPS than by ICP because the tin is segregated to the surface. The XPS and ICP results are presented in Figure 2.4.

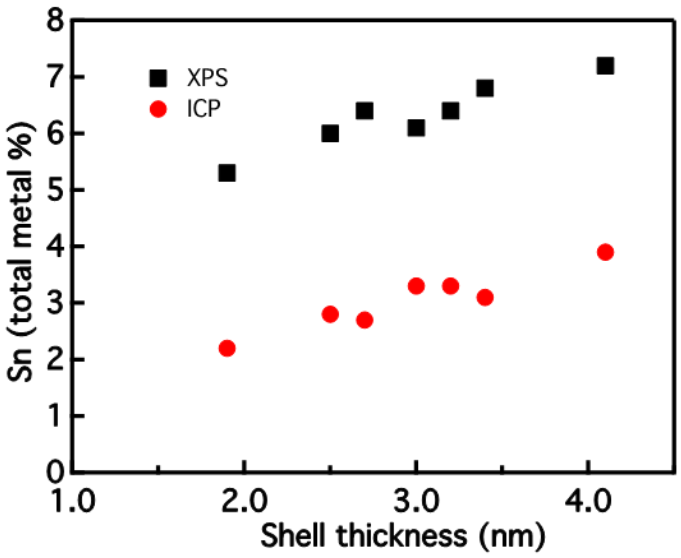

Figure 2.4 Tin doping by XPS and ICP. Tin concentration as measured by XPS and ICP. XPS results had higher concentrations measured compared to the ICP, which is consistent with IO/ITO core/shell NCs. (*XPS courtesy of Corey Staller*.)

The results from XPS and ICP are consistent with the synthesis of IO/ITO core/shell NCs. It is also important to note the increased difference between XPS and ICP data compared to the previous work, which suggest that better segregation of tin to the shell. This is attributed to the intermediate washing and removal of unreacted metal precursor after synthesizing the IO cores.

2.4 Optical spectra

Comparing the optical spectra of the core/shell NCs, the impact of dopant segregation on the LSPR can be observed. Dr. Ankit Agrawal simulated the optical spectra of the core/shell NCs, which are presented in Figure 2.5. The more intense peak behaves as expected. For increasing ITO shell thickness, a blue shift in LSPR and an increase in intensity is observed due to the increasing volume fraction of doped material. Similarly, in the core series, a red shift is LSPR and decrease in intensity is observed due to the increasing volume fraction of undoped material.

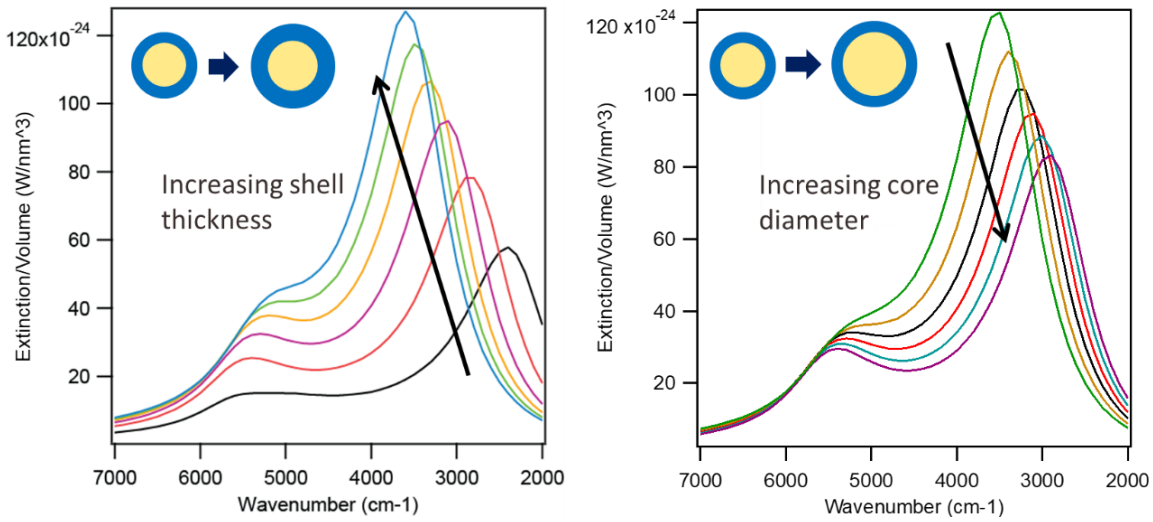

Figure 2.5 Simulated normalized optical spectra of core/shell NCs. Spectra for the core series and shell series show shifts in the LSPR frequency and changes in intensity corresponding to changing volume fraction of doped material. The dual mode in the LSPR calls for further investigation. *(Simulations courtesy of Dr. Ankit Agrawal.)*

Unexpectedly, there is a second mode in the LSPR at higher energies. This dual mode feature is currently under investigation. It is necessary to next collect the optical spectra of the synthesized core/shell NCs. This can be done by combined UV-vis and Fourier transform infrared (FTIR) spectroscopy measurements.

Chapter 3: Post-synthetic modulation of LSPR

3.1 Electrochemical modulation

The ability to dynamically modulate the LSPR frequency of ITO NCs opens opportunities for these materials in dynamic sensors. The carrier concentration in the material can be manipulated electrochemically by applying a bias. Recent work has demonstrated dynamic and reversible shifts in LSPR frequency of ITO NCs over a wide range.[10] Furthermore, as NFE is greatest at the LSPR frequency, the ability to tune the LSPR frequency to a target molecular vibration frequency can increase the coupling strength. These materials can be employed in a dynamic sensor in which LSPR frequency is electrochemically shifted to the frequency of target molecules. However, the NCs response to external stimuli is dependent upon the NC sensitivity to its surroundings. Improving sensitivity of the NCs is dependent upon understanding the impact of dopant

segregation on the depletion layer under bias. From analysis of the LSPR, reliable material properties can be extracted.[26]

By modeling the NCs in SCOUT, an optical spectra simulation and analysis software by W. Theiss, the relationship dopant segregation and depletion can be studied. In this chapter, a method for determining the change in the depletion layer thickness for IO/ITO core/shell NCs under an applied bias is described. The plasma frequency and damping parameter in the dielectric function given by the Drude model (Equation 1.1) can be extracted. Using Equation 1.2, the carrier concentration can also be calculated. Optical spectra of IO/ITO core/shell NCs collected over a voltage cycle were used to demonstrate this method. As shown in Figure 3.1, the NCs have a 16.3 nm diameter IO core and 4.1 nm thick ITO shell. The doping level in the shell was 5%. The IR spectra of the NCs were collected under bias, cycling from -1 V to 1 V to -1 V with a step size of 0.25 V, also shown in Figure 3.1. Modifying the model described by Agrawal et al. to account for the depletion layer, the simulated spectra are fit to the experimental spectra of these NCs.[24]

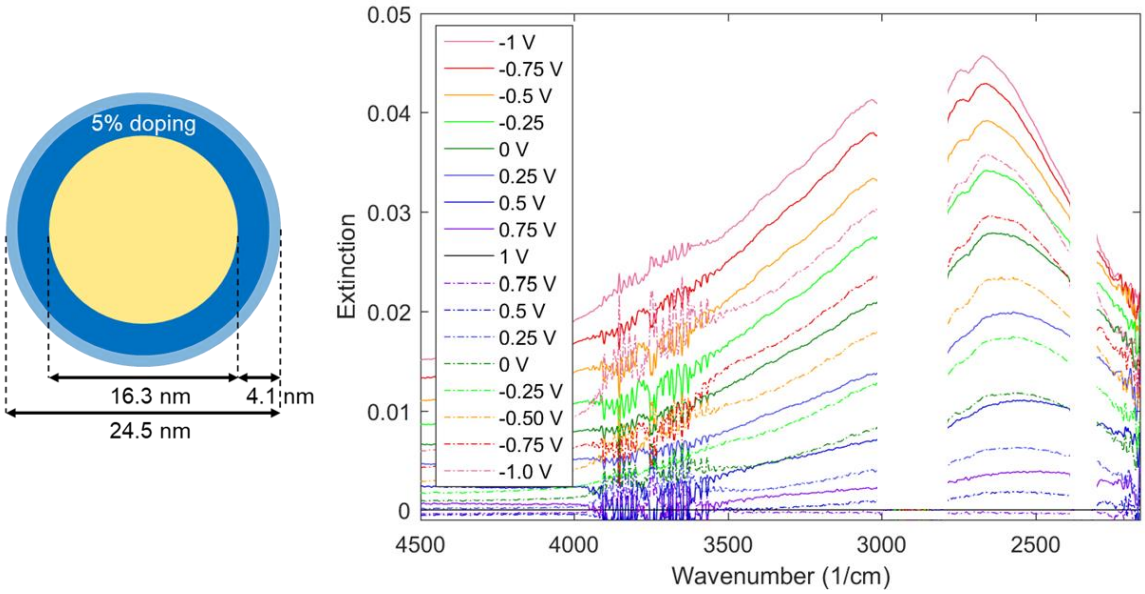

Figure 3.1 Optical spectra of core/shell NCs. (left) Illustration of IO/ITO core/shell NCs. (right) Background-subtracted IR spectra of core/shell NCs collected during a voltage cycle from -1 V to 1 V to -1 V. The ramp up is indicated by solid lines, and the ramp down is indicated by dashed lines. Measurements at equivalent voltages are in the same color. Hysteresis in optical spectra at equivalent voltages is observed. (*Materials and spectra courtesy of Bharat Tandon.*)

The spectra collected at the same voltage on the ramp up to 1 V and down to -1 V do not overlap, indicating hysteresis, which will affect the results of the fit. For improved measurements, the device should be cycled before spectra are collected.

To collect the optical spectra under bias, spectroelectrochemical (SEC) devices were assembled as described by Agrawal et al.[24] Films of the NCs form the working electrode, and Pt nanoclusters on ITO glass act as the counter electrode. The devices were connected

to a potentiostat, and *in situ* FTIR measurements were collected during a voltage cycle. Figure 3.2 illustrates device assembly.[24] Detailed device fabrication is described in the Appendix.

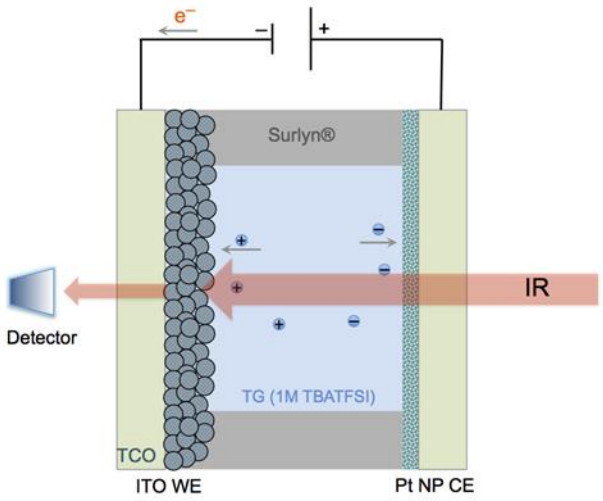

Figure 3.2 SEC Device assembly. The NC film is spun on glass as the working electrode. Pt nanoclusters on ITO glass is the counter electrode. The electrolyte is $TFSI^-$. Voltage is applied to the cell using a potentiostat, and optical spectra are collected using FTIR.[24]

The device components are included in the model in SCOUT to account for their optical contributions.

3.2 Modeling with SCOUT

The model of the device was built in SCOUT by defining the materials in the device and then stacking the materials in layers and defining layer thicknesses. In SCOUT, the NC films are defined in terms of volume fractions of the material in a matrix. The volume fraction of NCs in film can be obtained experimentally by measuring the film porosity using ellipsometric porosimetry (EP), but for now an estimate was made. In the device, the volume fraction of the NCs in the surrounding electrolyte is assumed to be 60% (or 40% porosity). The film thickness can also be measured experimentally, but it was assumed to be 60 nm for this exercise.

The core/shell/depletion layer structure is also defined in terms of volume fractions, where the IO core is in a ITO "matrix", which is in an IO "matrix". IO is used to model the depletion layer in SCOUT, assuming the depleted carrier concentration in the layer results in the material behaving like pure IO. The final modeled NC is in an electrolyte "matrix". However, as the depletion thickness changes under bias, the non-depleted ITO shell volume and depletion layer volume change. It is necessary to account for this relationship in SCOUT by employing master and slave parameters. To do this, consider the model of core/shell NCs in Figure 3.3.

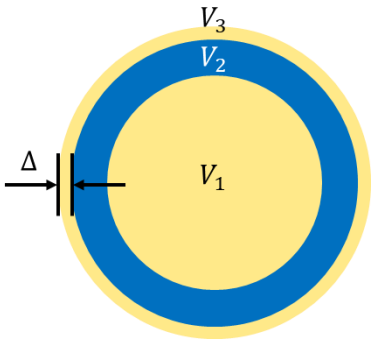

Figure 3.3 Model of core/shell NCs and the depletion layer. V_1 represents the IO core. V_2 is the non-depleted volume of the ITO shell plus the IO core, and V_3 is the total NC volume.

The volume fraction of IO in non-depleted ITO can be defined as V_{f1}, and the volume fraction of the NC in the total NC volume is V_{f2}, given by Equations 3.1 and 3.2:

$$V_{f1} = \frac{V_1}{V_2} \qquad \text{(Equation 3.1)}$$

$$V_{f2} = \frac{V_2}{V_3} \qquad \text{(Equation 3.2)}$$

where V_1 is the IO core volume, V_2 is the non-depleted NC volume, and V_3 is the total NC volume. Both the IO core volume and total NC volume can be determined from STEM images. Therefore, V_1/V_3 for the NCs can be calculated from experimental results, and the product of V_{f1} and V_{f2} can be used to relate the volume fractions in SCOUT.

$$V_{f1}V_{f2} = \frac{V_1}{V_2}\frac{V_2}{V_3} = \frac{V_1}{V_3} \qquad \text{(Equation 3.3)}$$

By defining a master parameter (V_m) and defining V_{f2} as a function of V_m, the volume fractions are coupled in SCOUT by the following equations:

$$V_m = V_{f1} \quad \text{(Equation 3.4)}$$

$$V_{f2} = \frac{\frac{V_1}{V_3}}{V_m} \quad \text{(Equation 3.5)}$$

The volume fraction of the IO core to the ITO shell, the volume fraction of the non-depleted NC to the total NC, the plasma frequency, and the damping parameter of the model were fit to the experimental spectra. Note that the optical response from electrolyte were omitted from the fit because the peaks occurred near the plasmon peak. The fitted volume fractions are plotted as a function of applied voltage in Figure 3.4. As the applied voltage is increased to 1 V, the electron concentration in the NCs is decreased, increasing the depletion layer thickness. As a result, the IO core becomes a larger volume fraction of the non-depleted shell V_2. This is reflected in the plot of V_{f1}, where the volume fraction increases for increasingly positive voltages. V_{f2} decreases with applied voltages approaching 1 V as expected due to the depletion layer thickness increasing and V_2 decreasing.

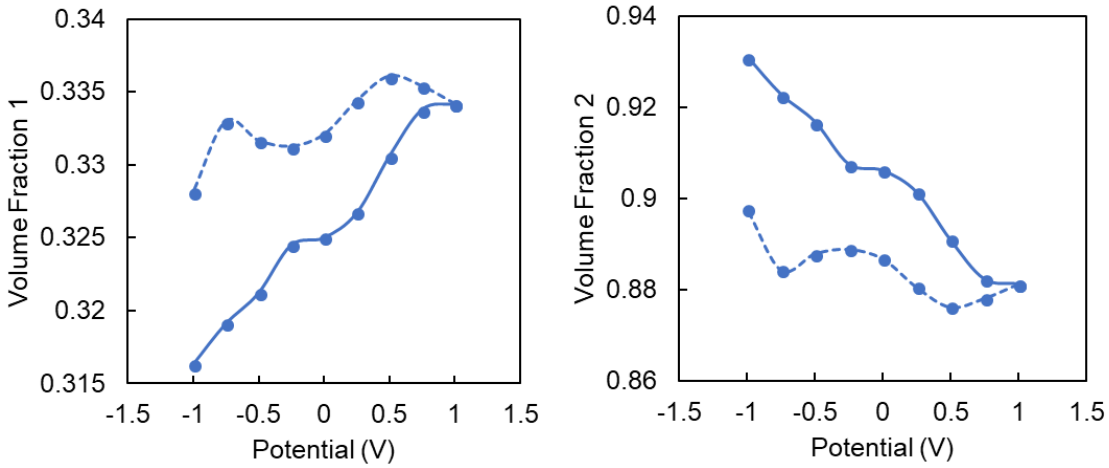

Figure 3.4 Volume fraction results. The solid line indicates the ramp up, and the dashed line indicates the ramp down. (left) The volume fraction of the undoped core to the non-depleted ITO shell (V_{f1}) increases and (right) the volume fraction of the non-depleted NC to the depleted shell (V_{f2}) decreases with more positive voltages due to the growing depletion layer thickness.

As shown in Figure 3.5, the plasma frequency is also shown to decrease (red shift) with increasing voltage due to the reduction in electron concentration. The damping increases with oxidation. Ideally, the parameter values extracted at -1 V at the start and end of the cycle would be equal. However, the values are not equal due to hysteresis, which was also observed in the optical spectra.

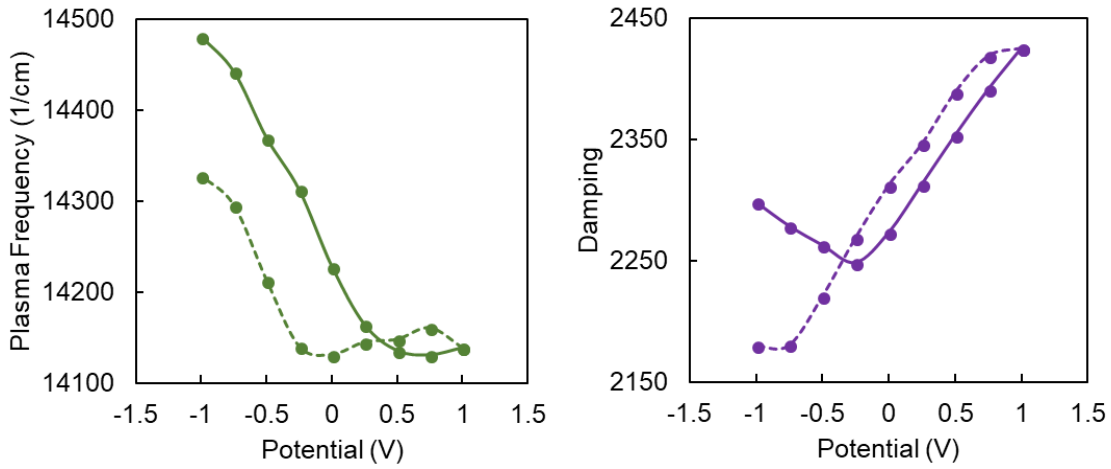

Figure 3.5 Model parameter results. The solid line indicates the ramp up, and the dashed line indicates the ramp down. (left) The plasma frequency decreases as the voltage increases to 1 V due to oxidation. (right) The damping parameter increases as the voltage increases to 1 V. The lack of agreement between parameters fit at the equivalent voltage after cycling indicates hysteresis.

From V_{f2} and the total NC volume, the depletion layer thickness can be calculated. The electron concentration can also be determined using Equation 1.2. In Figure 3.6, the depletion layer thickness and carrier concentrations are plotted as functions of applied voltage.

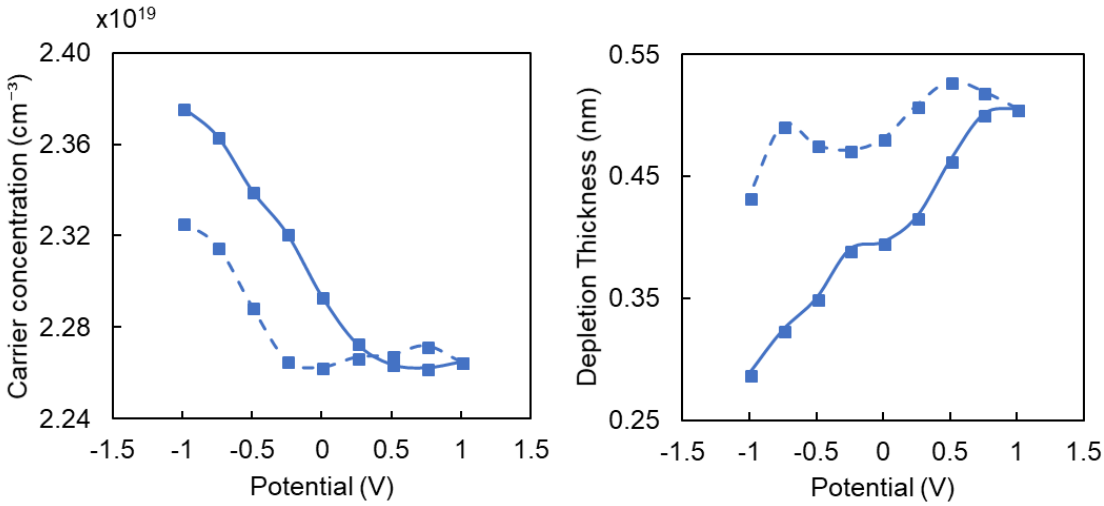

Figure 3.6 Extracted parameter results. The solid line indicates the ramp up, and the dashed line indicates the ramp down. The electron concentration (right) and depletion layer thickness (left) are plotted as a function of applied voltage. The depletion layer increases and the electron concentration decreases with increasing voltages due to the extraction of electrons.

The depletion layer increases with increasing voltage and the carrier concentration decreases due oxidation by the applied potential. Note that the depletion layer thickness is on a length-scale not negligible for nanoscale materials. Thus, this method can be used to extract the depletion layer thickness and carrier concentration of synthesized IO/ITO core/shell NCs.

Conclusions

Doped semiconductor NCs exhibit LSPR that can be tuned synthetically by changing the size and dopant concentration and electrochemically post-synthesis. The LSPR is in the near- to mid-IR region, allows sensing of molecular vibrations in this region. The plasmonic response also results in NFE that enables coupling between molecular vibrations and LSPR. However, sensitivity of the LSPR to the surroundings and NFE is reduced by the depletion layer that forms at the NC surface. Dopant segregation to the surface of the NC can reduce depletion by concentrating the electrons at the surface. The improved sensitivity is advantageous for applications requiring highly responsive materials, such as sensors.

To effectively segregate the dopants to the surface of the NC, independent control of the size and doping concentration is necessary. A slow growth synthesis procedure relying on the rapid esterification of metal oleates with oleyl alcohol to produce metal hydroxide and the subsequent condensation reaction enabled size control. Since the dopant precursor and indium oleate have similar reactivities, radial dopant distribution is also controlled, and improved dopant segregation is demonstrated. Using this procedure, IO/ITO core/shell NCs were synthesized. The synthesized series – the core series and the shell series – will enable study of the effect of increasing the ITO shell with a constant core volume and the effect of increasing the core volume with a constant shell thickness.

Simulated optical spectra indicated that with increasing ITO shell thickness, there is a blue-shift in the LSPR frequency due to the increasing volume fraction of doped material. With increasing IO core volume, there is a red-shift in the LSPR due to the reduced ITO volume fraction. Simulated results also reveal a dual mode LSPR; further investigation is necessary to fully understand the cause.

These NCs are a possible material for dynamic sensing. Electrochemical modulation of the LSPR can be demonstrated by applying a bias to the NCs. Analyzing the spectra under bias, the carrier concentration and the depletion layer thickness can be extracted, which can be used determine the impact of dopant segregation on these properties. The trends observed in the depletion layer thickness and carrier concentration are consistent with expectations for the change in applied voltage. The described method can be used to study synthesized core/shell NCs while accounting for depletion.

References

1. Agrawal, A.; Johns, R. W.; Milliron, D. J. Control of Localized Surface Plasmon Resonances in Metal Oxide Nanocrystals. *Annu. Rev. Mater. Res.* **2017,** 47, 1-31.
2. Abb, M.; Wang, Y.; Papasimakis, N.; de Groot, C. H.; Muskens, O. L. Surface-Enhanced Infrared Spectroscopy Using Metal Oxide Plasmonic Antenna Arrays. *Nano Lett.* **2014,** 14, 346-352.
3. Adato. R.; Atlug, H. In-Situ Ultra-Sensitive Infrared Absorption Spectroscopy of Biomolecule Interactions in Real Time with Plasmonic Nanoantennas. *Nat. Commun.* **2013,** 4, 2154.
4. Mendelsberg, R. J.; et al. Dispersible plasmonic doped metal oxide nanocrystal sensors that optically track redox reactions in aqueous media with single-electron sensitivity. *Adv. Opt. Mater.* **2015,** 3, 1293-1300.
5. Willets, K. A.; Van Duyne, R. P. Localized Surface Plasmon Resonance Spectroscopy and Sensing. *Annu. Rev. Phys. Chem.* **2007,** 58, 267-297.
6. Kundu, J.; Le, F.; Nordlander, P.; Halas, N. J. Surface Enhance Infrared Absorption (SEIRA) Spectroscopy on Nanoshell Aggregate Substrates. *Chem. Phys. Lett.* **2008,** 452, 115-119.
7. Stiles, P. L.; Dieringer, J. A.; Shah, N. C.; Van Duyne, R. P. Surface-Enhanced Raman Spectroscopy. *Annu. Rev. Anal. Chem.* **2008,** 1, 601-626.

8. Runnerstrom, E. L.; Llordes, A.; Lounis, S. D.; Milliron, D. J. Nanostructured Electrochromic Smart Windows: Traditional Materials and NIR-selective Plasmonic Nanocrystals. *Chemm. Commun.* **2014,** 50, 10555-10572.
9. Lounis, S. D.; Runnerstrom, E. L.; Bergerud, A.; Nordlund, D.; Milliron, D. J. Influence of Dopant Distribution on the Plasmonic Properties of Indium Tin Oxide Nanocrystals. *J. Am. Chem. Soc.* **2014,** 136, 7110-7116.
10. Garcia, G.; et al. Dynamically Modulating the Surface Plasmon Resonance of Doped Semiconductor Nanocrystals. *Nano Lett.* **2011,** 11, 4415-4420.
11. Haase, M.; Weller, H.; Henglein, A. Photochemistry and Radiation Chemistry of Colloidal Semiconductors. *J. Phys. Chem.* **1988,** 92, 482-487.
12. Valdez, C. N.; Braten, M.; Soria, A.; Gamelin, D. R.; Mayer, J. M. Effect of Protons on the Redox Chemistry of Colloidal Zinc Oxide Nanocrystals. *J. Am. Chem. Soc.* **2013,** 135, 8492-8495.
13. Schimpf, A. M.; Gunthardt, C. E.; Rinehart, J. D.; Mayer, J. M.; Gamelin, D. R. Controlling Carrier Densities in Photochemically Reduced Colloidal ZnO Nanocrystals: Size Dependence and Role of the Hole Quencher. *J. Am. Chem. Soc.* **2013,** 135, 16569-16577.
14. Lounis, S. D.; Runnerstrom, E. L.; Llordes, A.; Milliron, D. J. Defect Chemistry and Plasmon Physics of Colloidal Metal Oxide Nanocrystals. *J. Phys. Chem. Lett.* **2014,** 5, 1564-1574.

15. Bukasov, R.; Shumaker-Parry, J. S. Silver Nanocrescents with Infrared Plasmonic Properties as Tunable Substrates for Surface Enhanced Absorption Spectroscopy. *Anal. Chem.* **2009,** 81, 4531-4535.
16. Agrawal, A.; et al. Resonant Coupling between Molecular Vibrations and Localized Surface Plasmon Resonance of Faceted Metal Oxide Nanocrystals. *Nano Lett.* **2017,** 17, 2611-2620.
17. Agrawal, A.; et al. Rationalizing the Impact of Surface Depletion on Electrochemical Modulation of Plasmon Resonance Absorption in Metal Oxide Nanocrystals. *ACS Photonics.* **2018**.
18. Staller, C. M.; et al. Tuning Nanocrystal Surface Depletion by Controlling Dopant Distribution as a Route Toward Enhanced Film Conductivity. *Submitted* **2018.**
19. Ito, D.; Yokoyama, S.; Zaikova, T.; Masuko, K.; Hutchison, J. E. Synthesis of Ligand-Stabilized Metal Oxide Nanocrystals and Epitaxial Core/Shell Nanocrystals *via* a Lower-Temperature Esterification Process. *ACS Nano.* **2014,** 8, 64-75.
20. Jansons, A. W.; Hutchison, J. E. Continuous Growth of Metal Oxide Nanocrystals: Enhanced Control of Nanocrystal Size and Radial Dopant Distribution. *ACS Nano.* **2016,** 10, 6942-6951.
21. Crockett, B. M.; Jansons, A. W.; Koskelal, K. M.; Johnson, D. W.; Hutchison, J. E. Radial Dopant Placement for Tuning Plasmonic Properties in Metal Oxide Nanocrystals. *ACS Nano.* **2017,** 11, 7719-7728.

22. Mendelsberg, R. J.; Garcia, G.; Li, H.; Manna, L.; Milliron, D. J. Understanding the Plasmon Resonance in Ensembles of Degenerately Doped Semiconductor Nanocrystals. *J. Phys. Chem. C.* **2012,** 116, 12226-12231.
23. Agrawal, A.; Kriegel, I.; Milliron, D. J. Shape-Dependent Field Enhancement and Plasmon Resonance of Oxide Nanocrystals. *J. Phys. Chem. C.* **2015,** 119, 6227-6238.
24. Agrawal, A.*; Zandi, O.*; et al. Impacts of Surface Depletion on the Plasmonic Properties of Doped Semiconductor Nanocrystals. *Submitted* **2018.**
25. Kwon, S. G.; Hyeon, T. Formation Mechanisms of Uniform Nanocrystal via Hot-Injection and Heat-Up Methods. *Small.* **2011,** 7, 2685-2702.
26. Mendelsberg, R. J.; Garcia, G.; Milliron, D. J. Extracting Reliable Electronic Properties from Transmission Spectra of Indium Tin Oxide Thin Films and Nanocrystal Films by Careful Application of the Drude Theory. *J. Appl. Phys.* **2012,** 111, 063515.

Appendix

SEC device assembly

The spectroelectrochemical (SEC) device was assembled as described by Agrawal and Zandi, et al.[24] The NCs are spin-coated onto glass into a film to form the working electrode, and Pt nanoclusters are drop-cast onto an ITO/glass substrate to form the counter electrode. A polymer spacer with a punched hole is sandwiched between the two electrodes, and the space is filled with electrolyte (1 M $TFSI^-$) through pre-drilled holes in one of the electrodes. The holes are closed with epoxy, and copper tape is used to connect the electrodes to the potentiostat.

Tin concentration

Table A.1 Shell series size and tin concentration

Core Diameter (nm)	Shell Thickness (nm)	Shell Avg Sn%	XPS Sn%	ICP Sn%
15.8	1.9	4.6	5.3	2.2
16.5	2.5	5.2	6.0	2.8
16.1	3.4	4.8	6.8	3.1
16.3	4.1	5.6	7.2	3.9

Table A.2 Core series size and tin concentration

Core Diameter (nm)	Shell Thickness (nm)	Shell Avg Sn%	XPS Sn%	ICP Sn%
11.1	3.0	4.6	6.1	3.3
13.0	3.2	3.7	6.4	3.3
16.1	3.4	4.8	6.8	3.1
17.6	2.7	4.9	6.4	2.7

Raw SCOUT results

Table A.3 Parameter results by SCOUT fitting

Potential (V)	V_{f1}	V_{f2}	Damping	Plasma Frequency (cm^{-1})
-1.00	0.3163	0.9311	2298.325	14480.86
-0.75	0.3191	0.9228	2278.756	14442.11
-0.50	0.3212	0.9168	2262.906	14369.39
-0.25	0.3245	0.9075	2248.575	14312.15
0	0.3250	0.9061	2273.340	14227.84
0.25	0.3267	0.9014	2313.030	14163.94
0.50	0.3306	0.8909	2353.373	14135.26
0.75	0.3338	0.8823	2391.269	14130.65
1.00	0.3342	0.8812	2425.168	14138.56
0.75	0.3354	0.8781	2418.699	14160.51
0.50	0.3361	0.8762	2388.738	14147.94
0.25	0.3344	0.8806	2346.231	14144.83
0	0.3321	0.8868	2312.302	14131.26
-0.25	0.3313	0.8889	2268.999	14140.00
-0.50	0.3317	0.8879	2220.652	14212.84
-0.75	0.3330	0.8843	2180.518	14295.03
-1.00	0.3281	0.8976	2179.681	14327.55

Film porosity was assumed to be 40%, and film thickness was assumed to be 60 nm. To calculate the carrier concentration from the plasma frequency, $m^* = 0.4m_e$ where m_e is the mass of an electron.